



4-[[4-(Dimethylamino)benzylidene]amino]-5-methyl-4H-1,2,4-triazole-3-thiol as Corrosion Inhibitor for 316 Stainless Steel in 2.5 M Sulphuric Acid: An Experimental and Theoretical Investigation

N. SHET¹, R. NAZARETH¹, P. KRISHNA MURTHY²  and P.A. SUCHETAN^{3,*} 

¹Department of Chemistry, St. Aloysius College, Mangaluru-575003, India

²Department of Chemistry, Bapatla Engineering College (Autonomous), Acharaya Nagarjuna University Post Graduate Research Centre, Bapatla-522102, India

³Department of Studies and Research in Chemistry, University College of Science, Tumkur University, Tumkur-572103, India

*Corresponding author: E-mail: pasuchetan@gmail.com

Received: 1 October 2019;

Accepted: 8 November 2019;

Published online: 29 April 2020;

AJC-19828

The corrosion inhibition competence of 4-[[4-(dimethylamino)benzylidene]amino]-5-methyl-4H-1,2,4-triazole-3-thiol (DBTT) on 316 stainless steel (316 SS) in 2.5 M H₂SO₄ was studied using various electrochemical as well as weight-loss measurements. The alloy surface was examined by scanning electron microscopy (SEM) and energy dispersive X-ray spectroscopy (EDX). Concentration effect on inhibition efficiency was investigated by varying concentration from 5 to 2000 ppm in the temperature range 30-60 °C. Results indicated mixed-type inhibitory action of DBTT. The efficiency increased with the raise in concentration of DBTT and temperature, reaching a highest of 92.4 % at 60 °C. Langmuir adsorption isotherm is obeyed. Calculation of different thermodynamic factors suggests that the adsorption is *via* both physisorption and chemisorption. In addition to these, several global reactivity parameters were calculated using DFT method at B3LYP/6-311++(d,p) basis set. Theoretical calculations are in good concurrence with the experimental results.

Keywords: 316 Stainless steel, Sulphuric acid, Schiff base, Weight-loss method, Potentiodynamic Polarization, EIS, DFT calculations.

INTRODUCTION

Austenitic stainless steels have chromium and nickel as the main alloying elements and are well-known for their corrosion resistance. The resistance to corrosion attack originates from a thin passive surface layer rich in chromium and iron oxides. The presence of nickel in these alloys stabilizes the face-centred cubic austenite phase and enhances the corrosion resistance [1]. The austenitic stainless steels have been used extensively for architectural and industrial applications. Their corrosion resistance is further improved by the addition of 3 % molybdenum in type 316 stainless steels. This variety of steel can be used to contain corrosive chemicals including acids such as nitric acid and phosphoric acid. 316 SS is used for making specialized process equipment for food, paper, mining, pharmaceutical and petroleum industries [2]. However, 316 SS undergoes corrosion in the presence of chlorides which attack the passive layer and damage it. 316 SS is resistant to sulphuric acid at very low and very high concentrations but is attacked at intermediate concentrations.

Several methods have proved effective in reducing the corrosion of stainless steel. These include alloying [3,4], application of coatings [5,6] and use of inhibitors [7-15]. Both inorganic [7,8] and organic [9-12] compounds have been reported as corrosion inhibitors. Recently, eco-friendly chemicals such as amino acids, plant extracts and natural wastes have shown inhibitory actions [13-15].

Organic molecules used successfully as inhibitors are compounds with π -electrons and/or hetero atoms such as N, O, S or P. Heterocyclic compounds such as triazoles, thiazoles, imidazoles, pyridines, pyrimidines, *etc.* and their derivatives have exhibited excellent inhibiting action [16-20]. For instance, the inhibitory action of isoquinoline derivatives on 316L SS in H₂SO₄ was reported by Atta *et al.* [21]. 2-Mercaptobenzothiazole has been reportedly used as inhibitor for 316 SS in citric acid by Goudarzi *et al.* [22]. Moreira *et al.* [23] noticed the inhibitory behaviour of imidazole and benzimidazole on the corrosion of 316 SS in NaCl solution. According to a study conducted by Abdallah *et al.* [24], thiazole derivatives are efficient inhibitors for 316 SS in HCl medium.

These organic compounds adsorb on the metal surface and prevent the metal dissolution. The inhibitors may be classified as cathodic or anodic based on whether they affect cathodic process or anodic process. In many cases, the adsorption of inhibitors affects both cathodic and anodic processes although to different extents.

Schiff bases derived from triazoles have been tested as corrosion inhibitors for metals/alloys in various environments and are reported to exhibit excellent inhibiting action [25-27]. Further, inhibition effect shown by them is observed to be more than that of the constituent amines and aldehydes [28]. However, not much investigation is reported on the inhibiting action of Schiff bases on the corrosion of 316 SS. Therefore, in the present work, the corrosion inhibitory action of 4-[(dimethylamino)benzylidene]amino}-5-methyl-4*H*-1,2,4-triazole-3-thiol (DBTT) a Schiff base derived from triazole on the surface of 316 SS in 2.5 M H₂SO₄ medium is studied both experimentally and theoretically. The inhibition efficiency has been studied experimentally by means of potentiodynamic polarization, electrochemical impedance spectroscopy (EIS) and weight loss techniques and, theoretically by employing DFT method at B3LYP/6-311++(d,p) basis set.

EXPERIMENTAL

Inhibitor: The synthesis of DBTT inhibitor and its FT-IR spectrum has been already reported [29].

Medium: The experimental medium *i.e.*, 2.5 M H₂SO₄ was prepared from AR grade 98 % H₂SO₄ by dilution with double distilled water. Solutions with varying concentrations of the inhibitor (5 to 2000 ppm) were prepared by dissolving suitable amounts of DBTT in 2.5 M H₂SO₄. Electrochemical measurements were performed using 100 cm³ of each of these solutions, whereas, 200 cm³ were used for weight loss methods. All the solutions without de-aeration were employed. Calibrated thermostat was used to maintain constant temperature.

The 316 SS sample employed here contained (weight %): C 0.013 %, Mn 1.4 %, Si 0.3 %, S 0.001 %, P 0.026 %, Cr 17.2 %, Ni 10.18 %, Mo 2.1 %, N 0.026 % and Fe is the remainder.

Test coupon preparation: Test coupons required for the experiments were prepared as described earlier [29].

Weight-loss method: The test coupons were polished, cleaned, dried and weighed accurately using an analytical balance. The coupons were immersed in aggressive medium (2.5 M H₂SO₄ with or without different concentrations of DBTT) for different intervals of time (24-72 h) at 30 °C. They were removed from the solution, rinsed thoroughly with distilled water, followed by acetone, dried and weighed again. The weight differences prior to and after immersion in the medium were noted. The experiment was repeated thrice and the average weight-loss was calculated.

Electrochemical measurements: Electrochemical measurements were conducted using a three-electrode glass cell of 100 cm³ capacity, connected to GillAC (ACM instruments) electrochemical work-station (software version 5). Finely polished 316 SS coupon was made the working electrode, whereas, the reference and auxiliary electrodes were saturated calomel and platinum electrodes respectively. The electrodes were dipped in the corrosive medium (containing various

amounts of the inhibitor) and the open circuit potential (OCP) was monitored till a constant reading was attained. Electrochemical impedance spectra were then recorded followed by potentiodynamic polarization curves. The experiments were repeated at different temperatures (30-60 °C).

Impedance values were measured by applying perturbation of 10 mV sine-wave AC voltage at OCP in the frequency range of 100000 Hz to 0.01 Hz. The Nyquist plots were analyzed with the help of ZSimpwin 3.21 software.

The electrode potential was varied in the range of -250 mV to +250 mV with respect to OCP at a scan rate of 1 mV s⁻¹ for recording potentiodynamic polarization curves.

SEM-EDX studies: The surface characteristics of the 316 SS before and after exposure to corrosive medium were studied by means of SEM and EDX techniques. Polished and cleaned 316 SS coupons were dipped in 2.5 M H₂SO₄ devoid of or containing 500 ppm DBTT for 24 h. The coupons were then rinsed gently with distilled water, dried and images were recorded using a scanning electron microscope (Carl Zeiss). EDX profiles of the same surface were also recorded using an Energy dispersive X-ray analyser (Oxford Instruments).

Quantum chemical calculations: To estimate the electronic and reactivity properties of DBTT, the geometry was optimized in ground state in gas phase. All calculations were done within DFT with exchange correlation hybrid functional: B3LYP (three-parameter exchange functional of Becke B3 [30] combined with the Lee-Yang-Parr correlation functional LYP [31] using the extended basis sets with polarization and diffuse functions 6-311++G(d,p) by using Gaussian 09 software package [32]. For acuminous visualization, GaussView package was employed [33].

RESULTS AND DISCUSSION

Weight-loss experiment: 316 SS was dipped in a solution of 2.5 M H₂SO₄ in the absence and presence of DBTT of varied concentrations and the weight-losses were recorded at 30 °C. The experiment was recurred for different immersion times. The results are illustrated graphically in Fig. 1.

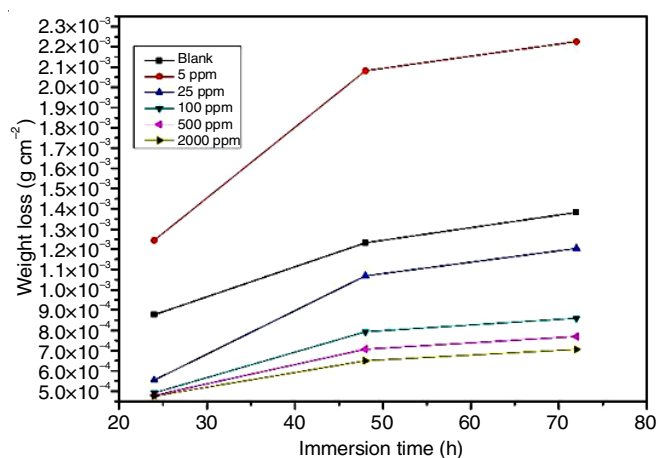


Fig. 1. Plot of weight-loss *versus* time for 316 SS in 2.5 M H₂SO₄ in the absence and presence of various concentrations of DBTT at 30 °C

It is noted that in the presence of the DBTT (except at 5 ppm concentration) at all immersion times the loss of weight

is significantly reduced than in the blank solution. Therefore, DBTT is an able corrosion inhibitor for 316 SS in 2.5 M H₂SO₄ medium. As [DBTT] increases, there is a greater decline in the weight-loss. Enhanced surface protection offered by the adsorbed DBTT molecules leading to lowering of reaction between the 316 SS surface and H₂SO₄ medium may be responsible for this. Inhibitor concentration of 5 ppm is probably less than the critical concentration of the inhibitor at this temperature and this leads to greater weight-loss in 5 ppm solution than the blank solution.

Eqn. 1 was used to calculate the corrosion rate [35].

$$CR_{wl} = \frac{K \cdot W}{A \cdot D \cdot T} \quad (1)$$

where, CR_{wl} is the corrosion rate (mm year⁻¹), W is the weight loss (mg), K = 87.6 (a constant), T is the exposure time (h), D is the density of the alloy (g cm⁻³) and A is the exposed surface area of the coupon to the medium (cm²).

The percentage inhibition efficiency was calculated using eqn. 2:

$$IE_{wl} (\%) = \frac{CR_{wl}^o - CR_{wl}}{CR_{wl}^o} \times 100 \quad (2)$$

where, CR_{wl}^o and CR_{wl} are respectively the rates of corrosion of the specimen immersed in acid solutions in absence and presence of DBTT for a given period.

CR_{wl} and IE_{wl} (%) obtained for different [DBTT] by varying the immersion time are given in Table-1.

TABLE-1 WEIGHT-LOSS STUDIES ON 316 SS IN 2.5 M H ₂ SO ₄ CONTAINING DIFFERENT CONCENTRATIONS OF DBTT AT 30 °C				
Immersion time (h)	Conc. of inhibitor (ppm)	Weight loss (mg cm ⁻²)	Corrosion rate (mm y ⁻¹)	Inhibition efficiency (%)
24	Blank	0.877	0.406	–
	5	1.244	0.576	–
	25	0.554	0.257	36.83
	100	0.491	0.227	44.03
	500	0.479	0.222	45.35
	2000	0.475	0.220	45.80
48	Blank	1.232	0.285	–
	5	2.082	0.482	–
	25	1.069	0.247	13.23
	100	0.792	0.183	35.67
	500	0.707	0.164	42.61
	2000	0.649	0.150	47.27
72	Blank	1.382	0.213	–
	5	2.226	0.344	–
	25	1.204	0.186	12.85
	100	0.860	0.133	37.73
	500	0.770	0.119	44.29
	2000	0.705	0.109	48.94

It is clear from Table-1 that for a particular period of immersion, there is a rise in IE_{wl} (%) with a rise in [DBTT]. This rise may be attributed to the enhanced adsorption of the DBTT molecules on the surface of 316 SS with the rise in concentration. However, no particular trend could be identified in the variation of inhibition efficiency with the immersion time. The inhibition efficiency increased slightly when the

immersion time varied from 24 to 72 h for solutions with inhibitor concentrations 500 ppm and more.

Potentiodynamic polarization studies: Fig. 2 illustrates the Tafel curves of 316 SS in 2.5 M H₂SO₄ in the absence and presence of different concentrations of DBTT at 40 °C.

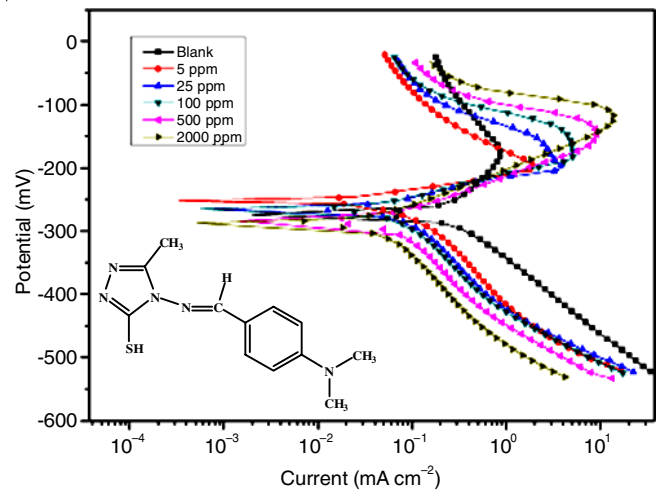


Fig. 2. Tafel polarization curves for 316 SS in 2.5 M H₂SO₄ with different concentrations of DBTT at 40 °C

Curves obtained at other temperatures were similar to these curves. As there was no linear Tafel region in the anodic polarization curve, corrosion current density i_{corr} was derived from the extrapolation of the cathodic part of the polarization curve to E_{corr} . The electrochemical parameters including corrosion current density i_{corr} , corrosion potential E_{corr} and cathodic slope β_c thus obtained are listed in Table-2.

The polarization curves shows that the presence of DBTT leads to a substantial decrease in the i_{corr} . However, at 30 °C, some increase in the i_{corr} was observed when [DBTT] = 5 ppm. Higher concentrations of DBTT led to greater decrease in i_{corr} . The addition of DBTT moved the cathodic polarization curves towards lower current density more than the anodic curves suggesting that DBTT strongly influences the cathodic reduction of H⁺ ions. This was affirmed by the observed shift of E_{corr} values in the negative direction. Nevertheless, these shifts were not significant enough to categorize DBTT as a cathodic inhibitor. An inhibitor can be classified as a cathodic or anodic inhibitor only when there is a shift of at least 85 mV in the corrosion potential [35]. Thus, DBTT may be regarded as a mixed-type inhibitor which shows predominant cathodic control. Besides, the cathodic curves obtained for the solutions with and without DBTT were almost parallel to each other with only little fluctuations in β_c values indicating that the cathodic reaction was suppressed without changing its mechanism [36]. This suggests that DBTT operates through simple blocking mechanism by getting adsorbed on the surface.

Eqn. 3 [37] was used to evaluate the corrosion rates.

$$v_{corr} = \frac{k \times E \times i_{corr}}{\rho} \quad (3)$$

where, k is a constant having value of 3270, E is the equivalent weight of the alloy, i_{corr} is the corrosion current density (mA

TABLE-2
 POTENTIODYNAMIC POLARIZATION STUDIES ON 316 SS IN 2.5 M H₂SO₄ CONTAINING DIFFERENT CONCENTRATIONS OF DBTT

Temp. (°C)	[DBTT] (ppm)	E _{corr} (mV/SCE)	i _{corr} (μA cm ⁻²)	-β _c (mV dec ⁻¹)	v _{corr} (mm y ⁻¹)	θ	IE (%)
30	0	-274.4	53.54	138.97	0.6503	–	–
	5	-270.8	59.64	150.76	0.7245	–	–
	25	-276.6	33.18	127.10	0.4030	0.3803	38.03
	100	-272.5	43.94	137.43	0.5337	0.1793	17.93
	500	-287.5	42.40	141.60	0.5150	0.2081	20.81
	2000	-296.8	37.23	146.33	0.4523	0.3045	30.45
35	0	-250.1	83.27	156.28	1.01146	–	–
	5	-245.3	69.71	169.92	0.8468	0.1628	16.28
	25	-261.5	60.63	156.86	0.7364	0.2719	27.19
	100	-264.2	58.06	169.43	0.7052	0.3028	30.28
	500	-275.9	54.82	170.36	0.6659	0.3416	34.16
	2000	-286.3	41.39	166.21	0.5028	0.5029	50.29
40	0	-274.5	258.02	119.04	3.1342	–	–
	5	-252.1	98.87	165.98	1.2009	0.6168	61.68
	25	-264.6	79.12	153.75	0.9611	0.6934	69.34
	100	-264.4	70.90	155.07	0.8612	0.7252	72.52
	500	-284.5	68.00	158.81	0.8260	0.7365	73.65
	2000	-287.8	49.35	162.87	0.5994	0.8088	80.88
50	0	-261.8	587.57	115.14	7.1372	–	–
	5	-250.1	126.60	148.93	1.5378	0.7845	78.45
	25	-265.8	142.07	146.25	1.7257	0.7582	75.82
	100	-265.9	127.14	151.25	1.5443	0.7836	78.36
	500	-282.1	98.51	156.71	1.1966	0.8323	83.23
	2000	-305.3	61.63	123.15	0.7486	0.8951	89.51
60	0	-257.4	1290.50	108.26	15.6756	–	–
	5	-253.3	269.99	117.31	3.2796	0.7908	79.08
	25	-264.6	240.52	141.87	2.9216	0.8136	81.36
	100	-266.7	181.69	148.84	2.2070	0.8592	85.92
	500	-289.4	124.49	135.92	1.5121	0.9035	90.35
	2000	-304.4	98.12	129.08	1.1918	0.9240	92.40

cm⁻²) and ρ is the density of the alloy (kg m⁻³) and v_{corr} is the corrosion rate (mm year⁻¹).

The inhibition efficiency IE_p (%) at different temperatures and different [DBTT] were determined from eqn. 4 [38]:

$$IE_p (\%) = \frac{v_{corr}^o - v_{corr}}{v_{corr}^o} \times 100 \quad (4)$$

where, v_{corr}^o and v_{corr} are respectively the corrosion rates in the absence and presence of DBTT.

The values of v_{corr} and IE_p (%) obtained by polarization studies are listed in Table-2. In the absence of DBTT, at low temperatures (30 and 35 °C), the corrosion rate of 316 SS in 2.5 M H₂SO₄ is similar to its corrosion rate in 2 M HCl (0.52 and 1.01 mm year⁻¹ at 30 and 35 °C respectively) reported in recent work [29]. At higher temperatures, however, 316 SS dissolution is much faster in 2.5 M H₂SO₄ than in 2 M HCl. In the presence of DBTT, the corrosion rate in 2.5 M H₂SO₄ is observed to be higher than that in 2 M HCl at all studied temperatures.

Further, it is evident from Table-2 that IE_p (%) increases with increasing [DBTT]. This may be the result of development of a barrier film which prevents the alloy surface from being attacked by the acid [39]. On comparison of these IE_p (%) values with those for the same inhibitor in 2 M HCl medium [29], we can deduce that DBTT exerts better inhibitive action in 2 M HCl than in 2.5 M H₂SO₄ (Maximum inhibition efficiency reported in 2 M HCl was 91.77 % at 50 °C with [DBTT] = 2000

ppm, whereas, in 2.5 M H₂SO₄ at the same temperature and inhibitor concentration, the efficiency is 89.51 %).

Effect of temperature: The effect of temperature on the rate of corrosion was studied in the range 30-60 °C. The corrosion rate showed an increase with the increasing temperature. This is due to the rise in conductivity of the medium with increase in temperature which further increases the rate of diffusion of H⁺ ions to the alloy surface [40]. Arrhenius equation (eqn. 5) [41] expresses the relation between rate of corrosion and temperature and is given as:

$$\ln v_{corr} = B - \frac{E_a}{RT} \quad (5)$$

where, B is a constant - whose value depends on the nature of the metal/alloy, R is the universal gas constant, T is the temperature and E_a is the apparent energy of activation of the reaction. Straight lines were obtained for ln v_{corr} vs. 1/T plots (Fig. 3a).

The slopes of these lines give the values of E_a (Table-3). The E_a values for inhibited solutions are lower than those for uninhibited solutions. The observed decrease in E_a values points towards low rate of adsorption of inhibitor at lower temperatures and this may be associated with chemisorption mechanism [42].

Activation parameters, ΔH[‡] and ΔS[‡] for the corrosion process were obtained with the help of transition state equation (eqn. 6) [43].

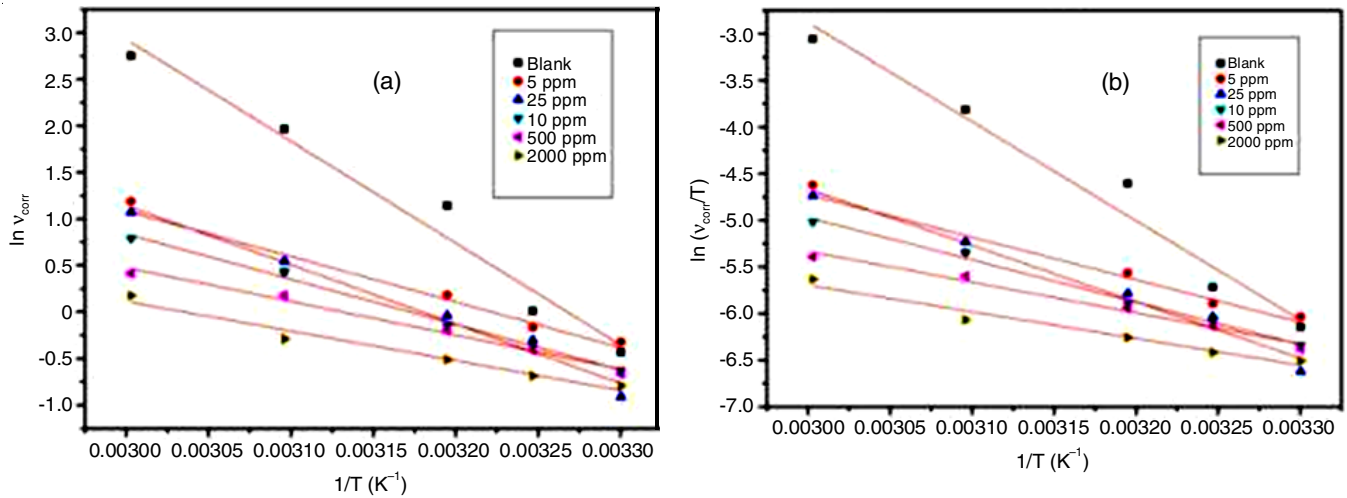


Fig. 3. Arrhenius plots (a) and transition state plots (b) for the corrosion of 316 SS in 2.5 M H₂SO₄ containing different concentrations of DBTT

TABLE-3
ACTIVATION PARAMETERS FOR THE DISSOLUTION OF 316 SS IN 2.5 M H₂SO₄ CONTAINING DIFFERENT CONCENTRATIONS OF DBTT

Concentration (ppm)	E _a (kJ mol ⁻¹)	ΔH [‡] (kJ mol ⁻¹)	ΔS [‡] (J mol ⁻¹ K ⁻¹)
0	90.97	88.33	43.50
5	40.66	38.02	-122.74
25	52.90	50.26	-85.56
100	40.45	37.80	-125.45
500	30.13	27.49	-159.41
2000	26.41	23.77	-173.57

$$\ln \frac{v_{\text{corr}}}{T} = \left[\ln \frac{R}{hN} + \left(\frac{\Delta S^{\ddagger}}{R} \right) \right] - \frac{\Delta H^{\ddagger}}{RT} \quad (6)$$

where, ΔS[‡] and ΔH[‡] are the entropy and enthalpy of activation respectively, h is Planck's constant and N is Avogadro's number.

Straight lines are obtained when ln (v_{corr}/T) is plotted against 1/T, -ΔH[‡]/R being the slope and (ln R/hN) + (ΔS[‡]/R) being the intercept (Fig. 3b).

Enthalpy and entropy of activation were calculated from the slope and the intercept respectively. Positive values of ΔH[‡] (Table-3) point out endothermic nature of the corrosion reaction. Further, negative sign of ΔS[‡] suggests decrease in system's disorder on departing from reactants to the activated complex in the presence of DBTT. Therefore, in the rate determining step, the activated complex formed should be as a result of association rather than dissociation [44].

Adsorption isotherm: Data obtained from potentiodynamic polarization studies were fitted graphically into various adsorption isotherms, namely, Langmuir, Temkin, Frumkin and Flory-Huggins. Since inhibitory action of organic inhibitors is through adsorption on the metal surface, the nature and extent of adsorption can be studied from these isotherms. Langmuir isotherm gives the best fit for the experimental data. Langmuir isotherm is given by the equation (eqn. 7) [45].

$$\frac{C_{\text{inh}}}{\theta} = \frac{1}{K_{\text{ads}}} + C_{\text{inh}} \quad (7)$$

In the above equation, C_{inh} stands for the concentration of the inhibitor in mol L⁻¹, K_{ads} is the equilibrium adsorption constant and θ is the degree of coverage of the surface by DBTT at different concentrations. Based on potentiodynamic polarization studies, θ was calculated with the help of eqn. 8:

$$\theta = \frac{IE_p(\%)}{100} \quad (8)$$

where, IE_p (%) is the inhibition efficiency. Straight lines at different temperatures were obtained for a plot of C_{inh}/θ vs. C_{inh}.

In each case, correlation coefficient (R²) was close to value of one indicating linearity relationship between the variables. The obedience of Langmuir's isotherm is generally associated with chemisorption [46]. The K_{ads} values were obtained from intercepts of these lines. At each temperature, standard free energy of adsorption ΔG^o_{ads} was calculated using eqn. 9 [46]:

$$\Delta G_{\text{ads}}^{\circ} = -RT \ln (55.5 K_{\text{ads}}) \quad (9)$$

where, 55.5 denotes the concentration of water in solution in mol L⁻¹. The K_{ads} and ΔG^o_{ads} values obtained are tabulated in Table-4.

TABLE-4
THERMODYNAMIC PARAMETERS FOR THE ADSORPTION OF DBTT ON 316 SS IN 2.5 M H₂SO₄ AT DIFFERENT TEMPERATURES

Temp. (°C)	K _{ads} (mol ⁻¹ L)	ΔG ^o _{ads} (kJ mol ⁻¹)	R ²	ΔH ^o _{ads} (kJ mol ⁻¹)	ΔS ^o _{ads} (J mol ⁻¹ K ⁻¹)
30	1.72 × 10 ³	-28.88	0.982		
35	2.24 × 10 ³	-30.04	0.983		
40	1.83 × 10 ⁴	-36.00	0.999	96.37	414.99
50	2.29 × 10 ⁴	-37.75	1.000		
60	5.21 × 10 ⁴	-41.19	1.000		

Higher temperature appears to favour stronger adsorption of the inhibitor as revealed by the increase in the K_{ads} values with the increase in temperature. At high temperature, the interaction between the alloy surface and the adsorbed molecules happens to be stronger, thereby, facilitating more adsorption. This elucidates the noted enhancement in inhibition efficiency with temperature and, also indicates that adsorption of the

inhibitor is by chemisorption. The values of K_{ads} obtained for the same inhibitor in 2 M HCl medium were much higher [29], implying a stronger adsorption of the inhibitor in 2 M HCl than 2.5 M H_2SO_4 .

Since all the $\Delta G_{\text{ads}}^\circ$ values are negative, it may be inferred that DBTT is spontaneously adsorbed on the steel surface forming a stable layer. Further, as temperature increases, adsorption is more favourable as the $\Delta G_{\text{ads}}^\circ$ becomes more negative at high temperatures [47]. The values of $\Delta G_{\text{ads}}^\circ$ range from approximately -28 to -41 kJ mol^{-1} , indicating that the adsorption of DBTT on 316 SS involves both physisorption and chemisorptions, with chemisorption being predominant [21]. Similar metal-inhibitor interaction was observed in 2 M HCl medium earlier [29].

According to eqn. 10 [48]:

$$\Delta G_{\text{ads}}^\circ = \Delta H_{\text{ads}}^\circ - T\Delta S_{\text{ads}}^\circ \quad (10)$$

where, $\Delta H_{\text{ads}}^\circ$ is standard enthalpy of adsorption and $\Delta S_{\text{ads}}^\circ$ is standard entropy of adsorption, the values of $\Delta G_{\text{ads}}^\circ$ were plotted against T to obtain a straight line.

Slope and intercept of the graph were used to derive the values of $\Delta S_{\text{ads}}^\circ$ and $\Delta H_{\text{ads}}^\circ$ values, respectively (Table-4). The adsorption here is an endothermic process which is evident from high positive value of $\Delta H_{\text{ads}}^\circ$ [49]. Further, this observation is consistent with the conclusions drawn with $\Delta G_{\text{ads}}^\circ$ and K_{ads} values that the adsorption involves chemisorption. $\Delta S_{\text{ads}}^\circ$ also has a high positive value which is due to the increase in disorder of the system during adsorption. This causes easy adsorption of DBTT.

EIS studies: EIS spectra of 316 SS immersed in uninhibited 2.5 M H_2SO_4 solution at 30 and 35 °C showed a semi-circular capacitive arc at high-frequency region followed by a Warburg tail at low-frequency region (Fig. 4a). The capacitive arc corresponds to the charge-transfer process across the oxide layer formed on the alloy surface whereas the low-frequency Warburg impedance suggests that the corrosion is limited by a diffusion process [50]. At higher temperatures (40 °C and above), the Warburg impedance was replaced by an inductive loop (Fig. 4b).

The EIS spectra of all inhibited solutions exhibited a well-defined capacitive arc at high frequency region and an inductive

loop at the low frequency region. The capacitive loop may be assigned to the charge-transfer between alloy and electrolyte whereas the inductive loop may be linked with the formation of Fe(I) and Fe(II) adsorbed intermediate species [51]. It may also be ascribed to the adsorption of inhibitor [52] or to the redissolution of the oxide-layer on the steel surface at low frequencies [53].

Another small inductive loop is observed at very high frequencies in some of the spectra which may be attributed to the actual physical inductance of the wires and possibly of the electrode itself [52]. The capacitive loops show a slightly depressed nature with their centres lying below the real axis which may be because of frequency dispersion. This is usually related with porous/heterogeneous nature of the electrode surface resulting in a diversion from ideal capacitive behaviour.

A large increase in impedance observed in inhibited solutions compared to blank solutions especially at high temperatures points out to strong inhibition of corrosion process, probably due to adsorption of the inhibitor on the alloy surface.

Equivalent circuits fitting the impedance data were obtained (Fig. 5a-c) using ZSimpwin 3.21 software and the parameters obtained are given in Table-5. The impedance data corresponding to the corrosion of 316 SS in 2.5 M H_2SO_4 without DBTT at low temperatures (30 and 35 °C) were analyzed in terms of the equivalent circuit presented in Fig. 5a. The circuit includes R_s , R_f , R_{ct} , C_f , Q_{dl} and W . R_s represents solution resistance, R_f and R_{ct} represent the resistance of the oxide film covering the alloy surface and charge-transfer resistance respectively. C_f represents the capacitance of the oxide film, Q_{dl} is a constant phase element denoting the double-layer and W is the Warburg element.

Equivalent circuit shown in Fig. 5b was used to fit the EIS results obtained for blank solution at higher temperatures (40 °C and above). The circuit consists of R_s , R_{ct} , Q_{dl} , R_f , Q_f (constant phase element corresponding to the oxide-film), L_1 and L_2 (inductive elements) and R_L (inductive resistance).

The results of EIS measurements of inhibited solutions were fitted using the equivalent circuit shown in Fig. 5c. The elements included in the circuit are R_s , R_{ct} , Q_{dl} , L_1 , L_2 and R_L .

In most places in these equivalent-circuits, an ideal capacitor was replaced by a constant phase element to obtain a better fit. At higher temperatures (40-60 °C), inhibited solutions show

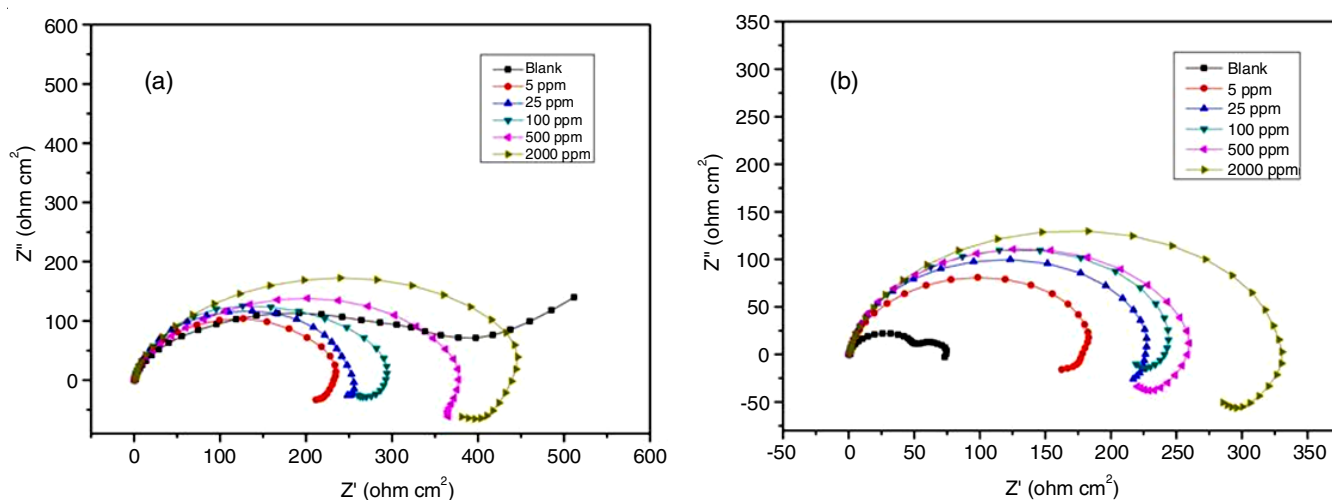


Fig. 4. Nyquist plots of 316 SS in 2.5 M H_2SO_4 with different concentrations of DBTT at (a) 35 °C and (b) 40 °C

TABLE-5
IMPEDANCE DATA FOR THE CORROSION OF 316 SS IN 2.5 M H₂SO₄ CONTAINING DIFFERENT CONCENTRATIONS OF DBTT

Temp. (°C)	[DBTT] (ppm)	R _{ct} (ohm cm ²)	Y _o × 10 ⁴ (S s ⁿ cm ⁻²)	n	C _{dl} × 10 ⁴ (F cm ⁻²)	IE (%)
30	Blank	531.1	5.90	0.544	2.55	–
	5	363.2	3.33	0.868	2.72	-46.23
	25	477.3	2.68	0.928	2.29	-11.27
	100	485.5	2.48	0.905	2.02	-9.39
	500	512.9	2.34	0.891	1.85	-3.55
	2000	523.7	1.82	0.863	1.29	-1.41
35	Blank	389.0	6.38	0.546	2.39	–
	5	159.9	2.54	0.942	2.16	-143.3
	25	182.2	3.08	0.924	2.54	-113.5
	100	236.8	2.00	0.928	1.59	-64.27
	500	367.9	2.43	0.869	1.75	-5.74
	2000	426.4	1.02	0.897	0.73	8.77
40	Blank	31.7	11.65	0.858	7.11	–
	5	131.6	3.32	0.926	2.70	75.88
	25	144.4	3.58	0.937	3.06	78.02
	100	155.5	3.23	0.914	2.54	79.59
	500	190.2	2.25	0.901	1.64	83.31
	2000	224.0	1.07	0.897	0.74	85.83
50	Blank	21.7	27.90	0.831	15.49	–
	5	92.8	5.51	0.907	4.11	76.61
	25	100.1	4.74	0.922	3.80	78.31
	100	108.2	5.32	0.874	3.57	79.94
	500	150.9	4.08	0.855	2.71	85.61
	2000	198.7	1.98	0.892	1.41	89.07
60	Blank	11.3	34.92	0.863	20.73	–
	5	49.6	18.44	0.813	8.49	77.28
	25	53.9	9.18	0.918	7.29	79.10
	100	65.3	5.69	0.900	4.15	82.74
	500	94.9	4.66	0.874	3.13	88.13
	2000	124.1	1.99	0.874	1.23	90.92

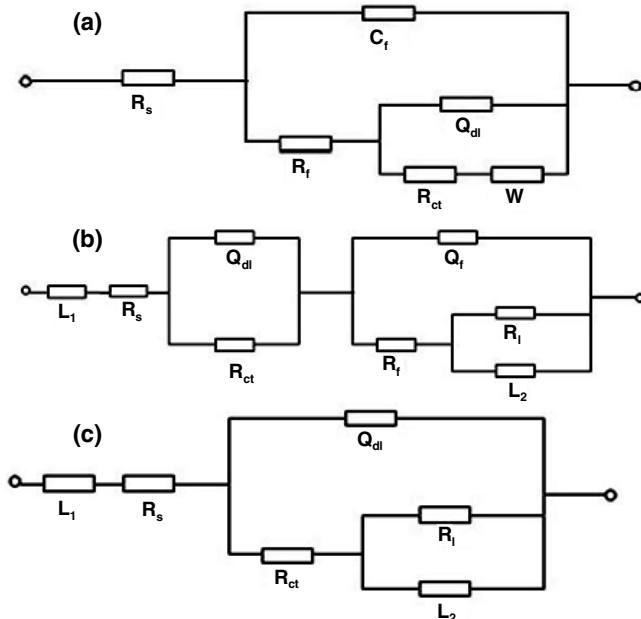


Fig. 5. Equivalent circuits used for fitting the EIS results of 316 SS in 2.5 M H₂SO₄ (a) at 30 and 35 °C in the absence of inhibitor (b) at 40, 50 and 60 °C in the absence of inhibitor and (c) in the presence of inhibitor at all temperatures

a greater charge-transfer resistance than uninhibited solutions (Table-5). Further, there is a steady increase in R_{ct} with the increase in [DBTT]. This may be due to the formation of a protective layer on the electrode surface, thereby, developing

a barrier for mass and charge-transfer [54]. R_{ct} is inversely proportional to corrosion current density *i*_{corr} (and thus to corrosion rate) as per the Stern-Geary equation (eqn. 11) [37]:

$$i_{\text{corr}} = \frac{\beta_a \beta_c}{2.303(\beta_a + \beta_c)R_{\text{ct}}} \quad (11)$$

Therefore, the increase in R_{ct} in the presence of the DBTT means decreased rate of corrosion.

However, at lower temperatures (30 and 35 °C), R_{ct} values shown by blank solution were higher than some of the inhibitor solutions. This is probably due to the stability of the passivating oxide-film at these temperatures. Higher temperatures increased the dissolution of the oxide layer causing a rapid increase in the corrosion rate.

Inhibition efficiency, IE_e (%) was calculated by using eqn. 12:

$$IE_e (\%) = \frac{R_{\text{ct}} - R_{\text{ct}}^0}{R_{\text{ct}}} \times 100 \quad (12)$$

where, R_{ct} and R_{ct}⁰ are the charge-transfer resistances in the presence and absence of the DBTT.

Double layer capacitance C_{dl}, was computed from circuit-fitting results using eqn. 13 [55]:

$$C_{\text{dl}} = Y_o (2\pi f_{\text{max}})^{n-1} \quad (13)$$

Here, Y_o is an admittance parameter, f_{max} is the frequency at which the imaginary component of the impedance has maximum value and n is the constant phase element exponent.

The values of C_{dl} at many temperatures displayed a steady decline with the increase in [DBTT]. Drop in C_{dl} value is a result of upsurge in the dielectric constant and/or an increase in the width of the electric double layer due to the adsorption of the DBTT [56]. Thus, reduction in C_{dl} values with the increasing [DBTT] implies that there is adsorption of the inhibitor at the metal-electrolyte interface and the degree of adsorption rises with the rise in [DBTT]. The approach of values of n to unity in the presence of DBTT indicates the enhancement of homogeneity of the surface owing to the adsorption of DBTT molecules [36].

SEM-EDX studies: The surfaces of the 316 SS samples were checked by SEM and EDX techniques to obtain a greater insight into the inhibition ability of DBTT. Fig. 6a-c displays the SEM images of the surfaces before exposure to 2.5 M H_2SO_4 and after immersion in 2.5 M H_2SO_4 in the absence and presence of 500 ppm of DBTT for 24 h at 30 °C. The surface of the freshly polished specimen is smooth without any pits and cracks (Fig. 6a). After immersion in 2.5 M H_2SO_4 , the surface has some pits and cracks due to corrosion (Fig. 6b). Later, in the presence of DBTT, the surface again appears uniform (Fig. 6c) as it is protected by a layer of DBTT molecules that suppresses the attack by 2.5 M H_2SO_4 .

EDX analyses were further carried out to identify the composition of the acid exposed metal surface in the absence and presence of DBTT. The corresponding data is presented in Table-6. The EDX spectrum of the freshly polished specimen (Fig. 7a) showed peaks corresponding to all major elements present in the alloy except molybdenum. But the EDX spectrum of the specimen immersed in blank 2.5 M H_2SO_4 (Fig. 7b) clearly showed the presence of molybdenum. This may be due to the formation of insoluble MoO_3 layer on the surface [51] as the dissolution of 316 SS progresses in sulphuric acid leading to substantial quantity of Mo on the surface. However, there was no peak representing Mo in the EDX profile of the sample surface exposed to the inhibitor solution (Fig. 7c). This suggests that the dissolution of surface is restricted in the presence of inhibitor.

Also, an examination of the EDX profile revealed a slight increase in the percentages of sulphur and nitrogen on the surface of the inhibited sample when compared to that of the freshly polished alloy and the alloy immersed in blank solution. This indicates that the corrosion inhibition is due to adsorption of DBTT molecules *via* sulphur- and nitrogen-containing sites.

Mechanism of corrosion inhibition: The Tafel studies have proved that DBTT is an inhibitor with predominant cathodic

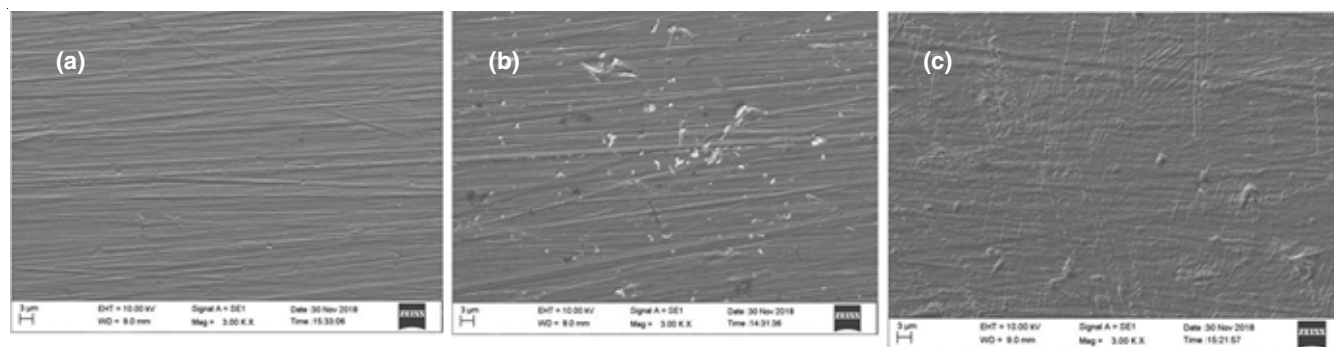


Fig. 6. SEM micrographs of (a) Freshly polished 316 SS (b) 316 SS exposed to 2.5 M H_2SO_4 in the absence of DBTT and (c) 316 SS exposed to 2.5 M H_2SO_4 in the presence of 500 ppm DBTT

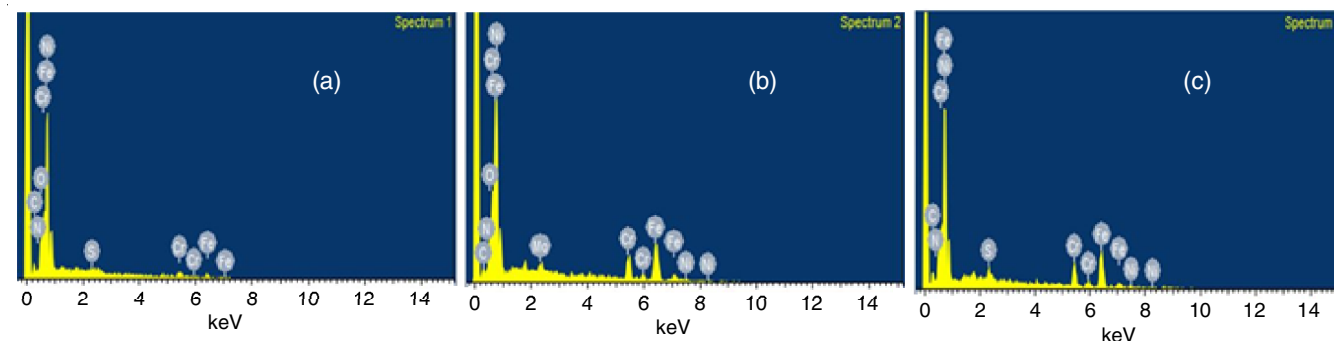
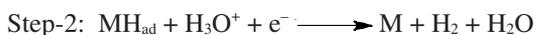
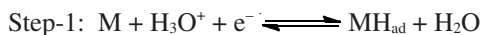


Fig. 7. EDX Spectra of 316 SS (a) freshly polished (b) exposed to 2.5 M H_2SO_4 in the absence of DBTT and (c) exposed to 2.5 M H_2SO_4 with 500 ppm DBTT

TABLE-6
EDX DATA OF 316 SS SURFACE UNDER DIFFERENT CONDITIONS

Element (Wt %)	C	N	O	S	Cr	Fe	Ni	Mo
Polished	1.32	0.31	1.33	0.36	16.22	65.53	14.93	–
Uninhibited	1.58	0.31	1.12	–	19.45	64.88	11.50	1.16
Inhibited	2.01	0.46	–	0.42	22.78	61.76	12.58	–

control. The cathodic protection by DBTT can be described on the basis of adsorption. DBTT gets adsorbed on the cathodic sites of the steel and thus decreases the hydrogen evolution reaction [17]. The mechanism proposed for the evolution of hydrogen in acidic media is as follows [21]:



Thus, the protonated inhibitor molecules compete with the H_3O^+ for adsorption on the alloy surface and thereby, deter the formation of MH_{ad} (Step-1). This in turn decreases the H_2 liberation by step 2 or 3.

Other factors, for instance, the nature of corrosive medium, the pH, the concentration of the inhibitor and the different functional groups present in the inhibitor will also influence the adsorption of a given inhibitor [13]. The hetero atoms of DBTT can act as active adsorption centres at the metal surface. The strength of adsorption is determined by the electron-density of the atoms and polarizability of the groups. The methyl groups present in the molecule are electron-donating and thus increase the localization of the lone-pair on nitrogen atoms. This enhances adsorption and subsequently corrosion inhibition [57].

Mode of adsorption: The adsorption of sulphate ions from the medium leads to the development of negative charge on the stainless steel surface. In H_2SO_4 solution, DBTT may exist either in the form of cations $DBTTH^+$ with a positive charge on nitrogen of the amino group or as neutral molecules. The neutral DBTT molecules get adsorbed on the steel surface displacing water molecules whereas the positively charged $DBTTH^+$ may be adsorbed through electrostatic interaction between positively charged N-atoms and the negatively charged alloy surface [58]. The mode of adsorption of DBTT and $DBTTH^+$ on steel surface is similar to the one described for HCl medium elsewhere [29]. The adsorption of DBTT on the electrode surface generates a barrier for transport of mass and charge. This leads to the shielding of the surface from the attack of aggressive ions.

However, at low concentrations of the inhibitor, the amount of DBTT is insufficient to cover the metal surface completely. As a result, the surface layer readily dissolves in the acidic environment. With the increase in concentration, more inhibitor molecules get adsorbed on the metal surface which subsequently reduces the solubility of the surface layer, leading to improved inhibiting effect.

Frontier molecular orbital analysis: Highest occupied molecular orbital (HOMO) energy depicts the electron donating capacity, while, energy of lowest unoccupied molecular orbital (LUMO) illustrates the electron accepting capacity. The combination of these two orbitals being called as Frontier molecular orbitals (FMOs). Therefore, higher energy value of HOMO suggests greater ability for electron(s) donation to the acceptor molecule with lower energy and empty molecular orbital [59], while, lower energy values of LUMO describes the electron accepting tendency of the [60,61]. The chemical behaviour of a molecule is better understood in terms of $\Delta E = E_{HOMO} - E_{LUMO}$. Further, the chemical reactivity of DBTT is described in terms

of various global reactivity parameters which were calculated by DFT method using B3LYP/6-311++g(d,p) basis set.

For DBTT, E_{HOMO} (MO: 69) and E_{LUMO} (MO: 70) values are -5.5081 and -1.5409 eV, respectively. The global chemical descriptors such as ionization potential $I = (-E_{HOMO})$, electron affinity $A = (-E_{LUMO})$, electronegativity $\chi = (I + A)/2$, global hardness $\eta = (I - A)/2$, chemical potential $\mu = -(I + A)/2$ and electrophilicity index, $\omega = (\mu^2/2\eta)$ [62] are calculated (Table-7). The HOMO-LUMO orbitals are shown in Fig. 8. The HOMO is confirmed over entire DBTT except the methyl group of triazole ring, whereas, the LUMO is confirmed over entire DBTT and partially on thiol and methyl groups.

TABLE-7
ENERGY VALUES OF DBTT CALCULATED
BY DFT/B3LYP/6-3++G(d,p) METHOD

Parameter	Gas phase (DFT/B3LYP/6-3++G(d,p))
SCF energy (a.u)	-1138.2134
E_{HOMO} (69) (eV)	-5.5081
E_{LUMO} (70) (eV)	-1.5409
$E_{HOMO} - E_{LUMO}$ (ΔE) (eV)	3.9600
Ionization potential ($I = -E_{HOMO}$)	5.5081
Electron affinity ($A = -E_{LUMO}$)	1.5409
Electronegativity ($\chi = (I + A)/2$)	3.5245
Global hardness ($\eta = (I - A)/2$)	1.9836
Chemical softness ($\nu = 1/\eta$)	0.5041
Chemical potential ($\mu = -(I + A)/2$)	-3.5245
Electrophilicity index ($\omega = \mu^2/2\eta$)	3.1312

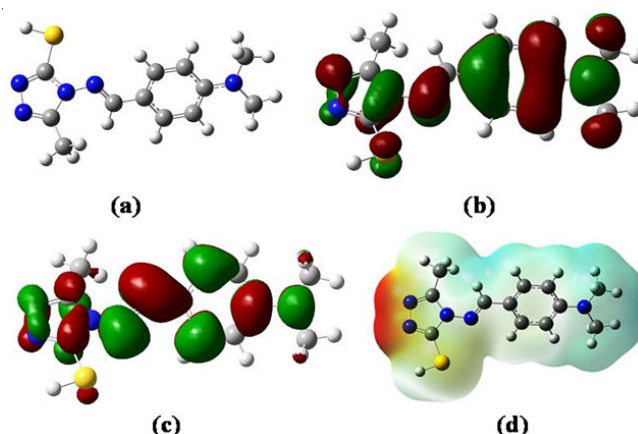


Fig. 8. (a) Optimized geometry, (b) HOMO, (c) LUMO, (d) electrostatic potential map of the title molecule

From the analysis of MEP (Fig. 8) and Mulliken atomic charges, it can be concluded that the electron rich regions have greatest ability to bind the metal surface (marked as red colour in MEP and represented with more negative value in Mulliken atomic charges), whereas, the electron poor regions have greatest ability to accept electrons (marked as blue regions in MEP as well as represented with positive value in Mulliken atomic charges). According to HSAB concept the hard acids tend to react with hard bases and soft acids actively react with soft bases. In the present case Fe (soft acid) reacts with nitrogen atoms (C=N) of triazole ring (soft base).

Summarizing the above results, it is concluded that the DBTT is able to give electrons to unoccupied d orbitals of metal

surface to form coordinate covalent bonds and can also accept free electrons from the metal surface by using their antibonding orbitals to form feedback bonds and thus, explaining its good corrosion inhibition property.

Conclusion

- 4-[[4-(Dimethylamino)benzylidene]amino]-5-methyl-4H-1,2,4-triazole-3-thiol (DBTT) is an effective corrosion inhibitor for 316 SS in 2.5 M H₂SO₄.
- DBTT exhibits mixed-type inhibition with predominant cathodic control.
- The inhibition efficiency enhances with the increase in [DBTT] and temperature.
- Inhibition is due to the adsorption phenomenon obeying Langmuir isotherm.
- Adsorption is through both physisorption and chemisorption but chiefly chemisorption.
- DBTT alters the surface morphology of 316 SS as evidenced by SEM-EDX studies.
- Results of potentiodynamic polarization and EIS methods are in concordance with the results of weight-loss method.
- Theoretical calculations accord the good inhibition efficiency of DBTT.

ACKNOWLEDGEMENTS

The authors are thankful to the Department of Chemistry, St. Aloysius College, Mangaluru, for providing laboratory facilities.

CONFLICT OF INTEREST

The authors declare that there is no conflict of interests regarding the publication of this article.

REFERENCES

1. D.A. Jones, Principles and Prevention of Corrosion, Pearson Education Limited: Essex, p. 516 (2014).
2. N. Goudarzi, M. Peikari, M.R. Zahiri and H.R. Mousavi, *Arch. Metall. Mater.*, **57**, 845 (2012); <https://doi.org/10.2478/v10172-012-0044-1>
3. W.-C. Chiang, I.-S. Tseng, P. Møller, L.R. Hilbert, T. Tolker-Nielsen and J.-K. Wu, *Mater. Chem. Phys.*, **119**, 123 (2010); <https://doi.org/10.1016/j.matchemphys.2009.08.035>
4. T. Sourisseau, E. Chauveau and B. Baroux, *Corros. Sci.*, **47**, 1097 (2005); <https://doi.org/10.1016/j.corsci.2004.05.024>
5. M.B. Gonzalez and S.B. Saidman, *Corros. Sci.*, **53**, 276 (2011); <https://doi.org/10.1016/j.corsci.2010.09.021>
6. P.A. Kilmartin, L. Trier and G.A. Wright, *Synth. Met.*, **131**, 99 (2002); [https://doi.org/10.1016/S0379-6779\(02\)00178-9](https://doi.org/10.1016/S0379-6779(02)00178-9)
7. M. Urgan and A.F. Cakir, *Corros. Sci.*, **32**, 835 (1991); [https://doi.org/10.1016/0010-938X\(91\)90028-N](https://doi.org/10.1016/0010-938X(91)90028-N)
8. H.A. El Dahan, *J. Mater. Sci.*, **34**, 851 (1999); <https://doi.org/10.1023/A:1004545501971>
9. L. Naravez, E. Cano and D.M. Bastidas, *J. Appl. Electrochem.*, **35**, 499 (2005); <https://doi.org/10.1007/s10800-005-0291-1>
10. A. Galal, N.F. Atta and M.H.S. Al-Hassan, *Mater. Chem. Phys.*, **89**, 38 (2005); <https://doi.org/10.1016/j.matchemphys.2004.08.019>
11. A.S. Fouda, M.A. Diab and S. Fathy, *Int. J. Electrochem. Sci.*, **12**, 347 (2017); <https://doi.org/10.20964/2017.01.60>
12. L.T. Popoola, *Corros. Rev.*, **37**, 71 (2019); <https://doi.org/10.1515/corrrev-2018-0058>
13. M. Yadav, T.K. Sarkar and T. Purkait, *J. Mol. Liq.*, **212**, 731 (2015); <https://doi.org/10.1016/j.molliq.2015.10.021>
14. N. Soltani, N. Tavakkoli, M. Khayatkashani, M.R. Jalali and A. Mosavizade, *Corros. Sci.*, **62**, 122 (2012); <https://doi.org/10.1016/j.corsci.2012.05.003>
15. O. Sanni, A.P.I. Popoola and O.S.I. Fayomi, *Results Phys.*, **9**, 225 (2018); <https://doi.org/10.1016/j.rinp.2018.02.001>
16. Z. Tao, S. Zhang, W. Li and B. Hou, *Corros. Sci.*, **51**, 2588 (2009); <https://doi.org/10.1016/j.corsci.2009.06.042>
17. L. Wang, M. Zhu, F. Yang and C. Gao, *Int. J. Corros.*, **2012**, 1 (2012); <https://doi.org/10.1155/2012/573964>
18. A.A. Al-Sarawy, A.S. Fouda and W.A.S. El-Dein, *Desalination*, **229**, 279 (2008); <https://doi.org/10.1016/j.desal.2007.09.013>
19. K.F. Khaled, *Electrochim. Acta*, **48**, 2493 (2003); [https://doi.org/10.1016/S0013-4686\(03\)00291-3](https://doi.org/10.1016/S0013-4686(03)00291-3)
20. M. Yadav, S. Yadav and A. Yadav, *J. Chem. Pharm. Res.*, **3/6**, 576 (2011).
21. N.F. Atta, A.M. Fekry and H.M. Hassaneen, *Int. J. Hydrogen Energy*, **36**, 6462 (2011); <https://doi.org/10.1016/j.ijhydene.2011.02.134>
22. N. Goudarzi and H. Farahani, *Anti-Corros. Methods Mater.*, **61**, 20 (2013); <https://doi.org/10.1108/ACMM-11-2012-1223>
23. R.R. Moreira, T.F. Soares and J. Ribeiro, *Adv. Chem. Eng. Sci.*, **4**, 503 (2014); <https://doi.org/10.4236/aces.2014.44052>
24. M. Abdallah, M.M. Salem, B.A.A.L. Jahdaly, M.I. Awad, E. Helal and A.S. Fouda, *Int. J. Electrochem. Sci.*, **12**, 4543 (2017); <https://doi.org/10.20964/2017.05.35>
25. D. Gopi, K.M. Govindaraju and L. Kavitha, *J. Appl. Electrochem.*, **40**, 1349 (2010); <https://doi.org/10.1007/s10800-010-0092-z>
26. Z. Zhang, L. Ruan, X. Huang, Y. Lyu, S. Zhang, W. Shang and X. Li, *Int. J. Electrochem. Sci.*, **12**, 576 (2017); <https://doi.org/10.20964/2017.01.37>
27. S. John, K.M. Ali and A. Joseph, *Bull. Mater. Sci.*, **34**, 1245 (2011); <https://doi.org/10.1007/s12034-011-0234-x>
28. M. Prajila and A. Joseph, *J. Mol. Liq.*, **241**, 1 (2017); <https://doi.org/10.1016/j.molliq.2017.05.136>
29. N. Shet, R. Nazareth and P.A. Suchetan, *Chem. Data Coll.*, **20**, 100209 (2019); <https://doi.org/10.1016/j.cdc.2019.100209>
30. A.D. Becke, *J. Chem. Phys.*, **98**, 5648 (1993); <https://doi.org/10.1063/1.464913>
31. C. Lee, W. Yang and R.G. Parr, *Phys. Rev. B Condens. Matter*, **37**, 785 (1988); <https://doi.org/10.1103/PhysRevB.37.785>
32. M.J. Frisch, G.W. Trucks, H.B. Schlegel, G.E. Scuseria, M.A. Robb, J.R. Cheeseman, G. Scalmani, V. Barone, B. Mennucci, G.A. Petersson, H. Nakatsuji, M. Caricato, X. Li, H.P. Hratchian, A.F. Izmaylov, J. Bloino, G. Zheng, J.L. Sonnenberg, M. Hada, M. Ehara, K. Toyota, R. Fukuda, J. Hasegawa, M. Ishida, T. Nakajima, Y. Honda, O. Kitao, H. Nakai, T. Vreven, J.A. Montgomery, Jr., J.E. Peralta, F. Ogliaro, M. Bearpark, J.J. Heyd, E. Brothers, K.N. Kudin, V.N. Staroverov, T. Keith, R. Kobayashi, J. Normand, K. Raghavachari, A. Rendell, J.C. Burant, S.S. Iyengar, J. Tomasi, M. Cossi, N. Rega, J.M. Millam, M. Klene, J.E. Knox, J.B. Cross, V. Bakken, C. Adamo, J. Jaramillo, R. Gomperts, O. Yazyev, R.E. Stratmann, A.J. Austin, R. Cammi, C. Pomelli, J.W. Ochterski, R.L. Martin, K. Morokuma, V.G. Zakrzewski, G.A. Voth, P. Salvador, J.J. Dannenberg, S. Dapprich, A.D. Daniels, O. Farkas, J.B. Foresman, J.V. Ortiz, J. Cioslowski and D.J. Fox, Gaussian, Inc., Wallingford CT, Gaussian 09, Revision B.01 (2010).
33. R. Dennington, T. Keith and J. Millam, Semichem Inc., Shawnee Mission KS, GaussView, Version 5 (2009).
34. M.G. Fontana, Corrosion Engineering, Tata McGraw Hill: New Delhi, p. 173 (2005).
35. A.K. Singh and M.A. Quraishi, *Int. J. Electrochem. Sci.*, **7**, 3222 (2012).
36. X. Zheng, M. Gong, Q. Li and L. Guo, *Sci. Rep.*, **8**, 9140 (2018); <https://doi.org/10.1038/s41598-018-27257-9>
37. B.S. Sanatkumar, J. Nayak and A.N. Shetty, *Chem. Sci. J.*, **2011**, 37 (2011).
38. F.M. Mahgoub, B.A. Abdel-Nabey and Y.A. El-Samadisy, *Mater. Chem. Phys.*, **120**, 104 (2010); <https://doi.org/10.1016/j.matchemphys.2009.10.028>
39. F. Bensajjay, S. Alehyen, M. El Achouri and S. Kertit, *Anti-Corros. Methods Mater.*, **50**, 402 (2003); <https://doi.org/10.1108/00035590310501558>

40. J. Fu, J. Pan, Z. Liu, S. Li and Y. Wang, *Int. J. Electrochem. Sci.*, **6**, 2072 (2011).
41. N. Dinodi and A.N. Shetty, *Corros. Sci.*, **85**, 411 (2014); <https://doi.org/10.1016/j.corsci.2014.04.052>
42. A.A. Atia and M.M. Saleh, *J. Appl. Electrochem.*, **33**, 171 (2003); <https://doi.org/10.1023/A:1024083117949>
43. Y.H. Ahmad and W.M.I. Hassan, *Int. J. Electrochem. Sci.*, **7**, 12456 (2012).
44. P. Kumari, P. Shetty and S.A. Rao, *Int. J. Corros.*, **2014**, 1 (2014); <https://doi.org/10.1155/2014/256424>
45. E.A. Noor, *Mater. Chem. Phys.*, **114**, 533 (2009); <https://doi.org/10.1016/j.matchemphys.2008.09.065>
46. M. Bouklah, N. Benchat, B. Hammouti, A. Aouniti and S. Kertit, *Mater. Lett.*, **60**, 1901 (2006); <https://doi.org/10.1016/j.matlet.2005.12.051>
47. K.C. Emregul and M. Hayvali, *Corros. Sci.*, **48**, 797 (2006); <https://doi.org/10.1016/j.corsci.2005.03.001>
48. H. Jafari, I. Danaee, H. Eskandari and M. RashvandAvei, *J. Mater. Sci. Technol.*, **30**, 239 (2014); <https://doi.org/10.1016/j.jmst.2014.01.003>
49. T. Poornima, J. Nayak and A.N. Shetty, *J. Appl. Electrochem.*, **41**, 223 (2011); <https://doi.org/10.1007/s10800-010-0227-2>
50. S.V. Lamaka, M.L. Zheludkevich, K.A. Yasakau, M.F. Montemor and M.G.S. Ferreira, *Electrochim. Acta*, **52**, 7231 (2007); <https://doi.org/10.1016/j.electacta.2007.05.058>
51. A. Pardo, M.C. Merino, A.E. Coy, F. Viejo, R. Arrabal and E. Matykina, *Corros. Sci.*, **50**, 780 (2008); <https://doi.org/10.1016/j.corsci.2007.11.004>
52. N. Labjar, M. Lebrini, F. Bentiss, N. Chihib, S.E. Hajjaji and C. Jama, *Mater. Chem. Phys.*, **119**, 330 (2010); <https://doi.org/10.1016/j.matchemphys.2009.09.006>
53. H.H. Hassan, E. Abdelghani and M.A. Amin, *Electrochim. Acta*, **52**, 6359 (2007); <https://doi.org/10.1016/j.electacta.2007.04.046>
54. M. Behpour, S.M. Ghoreishi, N. Mohammadi and M. Salavati-Niasari, *Corros. Sci.*, **53**, 3380 (2011); <https://doi.org/10.1016/j.corsci.2011.06.017>
55. T. Poornima, J. Nayak and A.N. Shetty, *J. Metall.*, **2012**, 1 (2012); <https://doi.org/10.1155/2012/723687>
56. P.C. Okafor, X. Liu and Y.G. Zheng, *Corros. Sci.*, **51**, 761 (2009); <https://doi.org/10.1016/j.corsci.2009.01.017>
57. M. Abdallah, *Mater. Chem. Phys.*, **82**, 786 (2003); [https://doi.org/10.1016/S0254-0584\(03\)00367-5](https://doi.org/10.1016/S0254-0584(03)00367-5)
58. S.A. Abd El-Maksoud, *Appl. Surf. Sci.*, **206**, 129 (2003); [https://doi.org/10.1016/S0169-4332\(02\)01188-1](https://doi.org/10.1016/S0169-4332(02)01188-1)
59. P. Udhayakala, T.V. Rajendiran and S. Gunasekaran, *Int. J. Adv. Sci. Res.*, **3**, 67 (2012).
60. J. Fang and J. Li, *J. Mol. Struct. THEOCHEM*, **593**, 179 (2002); [https://doi.org/10.1016/S0166-1280\(02\)00316-0](https://doi.org/10.1016/S0166-1280(02)00316-0)
61. E.E. Ebenso, D.A. Isabirye and N.O. Eddy, *Int. J. Mol. Sci.*, **11**, 2473 (2010); <https://doi.org/10.3390/ijms11062473>
62. R. Parr, L. Szentpaly and S. Liu, *J. Am. Chem. Soc.*, **121**, 1922 (1999); <https://doi.org/10.1021/ja983494x>